

Simulation of laboratory accretion disk and weakly ionized hypersonic flows using Nautilus

John Loverich, Ammar Hakim, Sudhakar Mahalingam, Peter Stoltz, Sean C.D. Zhou
Tech-X Corporation

Michael Keidar, Mahdu Kandrapu and TaiSen Zhuang
George Washington University

Jason Cassibry and Richard Hatcher
University of Alabama

A proposed experiment at HyperV technologies in partnership with Los Alamos National Lab will explore the use of merging, high velocity (50km/s) plasma jets as a laboratory model for astrophysical accretion disks. Similarly, researchers at George Washington University (GWU) are currently developing an experiment for investigating weakly ionized hypersonic flow in magnetic fields. The two experiments cover a broad range of hypersonic conducting fluid flows which can be explored using the shock capturing plasma fluid code, Nautilus.¹ In this paper, progress on modeling both experiments is presented along with associated physics and numerical techniques.

I. Introduction

Nautilus (<http://nautilus.txcorp.com>) is a flexible fluid plasmas code under development at Tech-X corporation. It solves a variety of fluid and fluid plasma systems including Navier Stokes, various forms of MHD including two-temperature and Hall MHD, fully electromagnetic multi-fluid plasma models and 10 moment extensions. This paper describes a few of the high density plasma models implemented in Nautilus and recent applications of the code in support of the PLX^{2,3} and development of the code for modeling re-entry vehicles to help develop tools to investigate blackout mitigation, the latter work being performed in conjunction with Michael Keidar's group (<http://cobweb.seas.gwu.edu/~mpnl>) at George Washington University. In addition, the flexibility of the code means that multiple systems can be solved (and coupled through source terms) in a single simulation. In particular this allows for the representation of a neutral species using Navier Stokes equations combined with an ionized species using the MHD equation and coupled through user specified collisional source terms. This capability allows the user to define complex systems such as weakly ionized plasmas in strong magnetic fields which has applications to radio blackout mitigation of hypersonic vehicles.

II. Equations

The system of equations used in these simulations are the various forms of the MHD equations with finite rate chemistry. The plasma jets problem is solved only using real gas equations of state while the hypersonic shock modeling problems are solved using a 7 or 11 component air chemistry model with NASA thermobuild equations of state. The following systems are solved using a positivity preserving MUSCL algorithm.

- **Reacting Navier Stokes**

$$\frac{\partial}{\partial t} \begin{pmatrix} \rho \\ \rho u_x \\ \rho u_y \\ \rho u_z \\ e \end{pmatrix} + \nabla \cdot \begin{pmatrix} \rho u_x & \rho u_y & \rho u_z \\ \rho u_x^2 + P & \rho u_x u_y & \rho u_x u_z \\ \rho u_y u_x & \rho u_y u_y + P & \rho u_y u_z \\ \rho u_z u_x & \rho u_z u_y & \rho u_z u_z + P \\ u_x (e + P) & u_y (e + P) & u_z (e + P) \end{pmatrix} = \dots \quad (1)$$

- **MHD in conservative form**

$$\frac{\partial}{\partial t} \begin{pmatrix} \rho \\ \rho u_x \\ \rho u_y \\ \rho u_z \\ e \\ B_x \\ B_y \\ B_z \end{pmatrix} + \frac{\partial}{\partial x} \begin{pmatrix} \rho u_x \\ \rho u_x^2 + P - \frac{1}{2\mu_0} B_x^2 + \frac{1}{\mu_0} B^2 \\ \rho u_y u_x - \frac{1}{\mu_0} B_x B_y \\ \rho u_z u_x - \frac{1}{\mu_0} B_x B_z \\ u_x (e + P + \frac{1}{2\mu_0} B^2) - \frac{1}{\mu_0} B_x B \cdot u \\ 0 \\ -E_z \\ E_y \end{pmatrix} + \frac{\partial F_y}{\partial y} + \frac{\partial F_z}{\partial z} = \dots \quad (2)$$

- **MHD in gas dynamic form**

$$\frac{\partial}{\partial t} \begin{pmatrix} \rho \\ \rho u_x \\ \rho u_y \\ \rho u_z \\ e \\ B_x \\ B_y \\ B_z \end{pmatrix} + \frac{\partial}{\partial x} \begin{pmatrix} \rho u_x \\ \rho u_x^2 + P \\ \rho u_y u_x \\ \rho u_z u_x \\ u_x (e + P) \\ 0 \\ -E_z \\ E_y \end{pmatrix} + \frac{\partial F_y}{\partial y} + \frac{\partial F_z}{\partial z} = \begin{pmatrix} 0 \\ J_y B_z - J_z B_y \\ J_z B_x - J_x B_z \\ J_x B_y - J_y B_x \\ E \cdot J \\ 0 \\ 0 \\ 0 \end{pmatrix} + \dots \quad (3)$$

In all cases the different fluid models can be simulated with an arbitrary number of continuity equations representing different species

$$\frac{\partial n_i}{\partial t} + \nabla \cdot [n_i u] = S \quad (4)$$

In the case of reacting flow S is determined from a set of rate equations. In all cases the pressure P can be calculated using an arbitrary equation of state. The pressure P is currently calculated using either NASA Thermobuild (for chemically reacting flows), SESAME or PROPACEOS (from Prism Computational Sciences <http://www.prism-cs.com/Software/PROPACEOS/PROPACEOS.htm>) tables.

III. Numerical Approach

In simulations that have an imposed magnetic field in addition to an induced magnetic field a slightly different algorithm is used. In this case the imposed field B_0 is not evolved, but the induced field \tilde{B} is. The total field is simply $B = B_0 + \tilde{B}$. When solving the MHD equation in conservative form we split the vector of conserved variables q into the time dependent and non time dependent parts so that $q = q_0 + \tilde{q}$ with

$$\tilde{q} = \begin{pmatrix} \rho \\ \rho u_x \\ \rho u_y \\ \rho u_z \\ e_{int} + \frac{1}{2} \rho u \cdot u + \frac{1}{2\mu_0} [\tilde{B} \cdot \tilde{B} + 2\tilde{B} \cdot B_0] \\ \tilde{B}_x \\ \tilde{B}_y \\ \tilde{B}_z \end{pmatrix} \quad \text{and} \quad q_0 = \begin{pmatrix} 0 \\ 0 \\ 0 \\ 0 \\ \frac{1}{2\mu_0} B_0 \cdot B_0 \\ B_{0x} \\ B_{0y} \\ B_{0z} \end{pmatrix} \quad (5)$$

The conservation law is then solved in the form

$$\frac{\partial \tilde{q}}{\partial t} + \nabla \cdot f(q) = S(q) \quad (6)$$

When the MHD equation are written in gas dynamic form with S containing $J \times B$ and $E \cdot J$ the energy term in q_0 is zero as well. The advantages of the split field formulation is that numerical diffusion tends to move the magnetic field to the imposed background value B_0 instead of moving it to zero, in addition, when using hyperbolic divergence cleaning (as described below) less diffusion of the field is observed.

The simulations performed in this paper used positivity preserving MUSCL algorithms in Nautilus. The simple approach requires one to use a positivity conserving flux such as the HLLC, HLLC or the local Lax flux to compute interface fluxes, limiters are applied once, then anywhere negative densities or pressures are calculated during interpolation to the faces the solution in that cells is set to first order. A less diffusive approach for the ideal MHD equations is described by Waagan in.⁴

In the MHD solvers the fields were solved using a modified form of the hyperbolic divergence cleaning technique. Hyperbolic divergence cleaning for the MHD equations was first described by Dedner.⁵ For our particular system we split the hyperbolic algorithm into two separate steps. In the first step the MHD equations are solved. In the second step the hyperbolic divergence equations are solved to propagate errors in $\nabla \cdot B$ out of the domain at finite speed.

- **step 1:**

Solve the hyperbolic system ignoring divergence corrections.

$$\frac{\partial q}{\partial t} + \nabla \cdot f(q) = S \quad (7)$$

- **step 2:**

Solve the correction system to move the error out of the domain at finite speed. This approach can be used for all sorts of systems that have a divergence constraint including MHD, two-fluid and Maxwell's equations.

$$\frac{\partial B}{\partial t} + \nabla \psi = 0 \quad (8)$$

$$\frac{\partial \psi}{\partial t} + \Gamma^2 \nabla \cdot B = 0 \quad (9)$$

for systems decomposed into static and perturbed magnetic fields this equation becomes

$$\frac{\partial \tilde{B}}{\partial t} + \nabla \psi = 0 \quad (10)$$

$$\frac{\partial \psi}{\partial t} + \Gamma^2 \nabla \cdot \tilde{B} = 0 \quad (11)$$

so that the divergence cleaning is only applied to the perturbed field.

IV. Accretion disk problem

The Plasma Liner Experiment² (PLX) at Los Alamos National Laboratory is a new experiment to explore high energy density plasma regimes. The experiment consists of a 9 foot diameter spherical tank with ports for 30 plasma jets. HyperV Technologies Corporation (<http://www.hyperv.com>) has been contracted to build the plasma jets⁶ and investigate smaller scale experiments inside their laboratory. One of these investigations will be the laboratory accretion disk experiment.

The laboratory accretion disk experiment is a concept originally described by Dimitre Ryutov⁷ and the same concept using laser generated plasmas in a second paper.⁸ The experiment would allow the laboratory investigation of astrophysical accretion disks. The setup is quite simple, a series of high mach number plasma jets (in this case mach 10) arrayed in a circle are directed towards, but slightly offset from the origin. In addition a pair of coils above and below the plane of the jets are used to set up a cusp magnetic field. The coils have oppositely directed currents so that the cusp field is set up.

As a first step an accretion disk simulation has been performed without the cusp field. Jet nozzle exit is 2cm diameter, jet exit velocity is 50km/s jet species is argon, jet pulse length is 5.0 microseconds, initial jet

temperature is 3eV, argon number density in the jet is $1 \times 10^{22}/m^3$. Figures 1 2 3 illustrates the arrangement of the jets and the resulting accretion disk formation without magnetic fields. These simulations used 12 jets and showed that a rotating disk of gas forms, and expands. When viscous and thermal terms are ignored, no gas penetrates the center of the ring. The gas the expands radially and axially. It's hoped that the introduction of a magnetic field will help to confine this radial expansion and mimic collimated plasma jets observed emanating from astrophysical accretion disks.

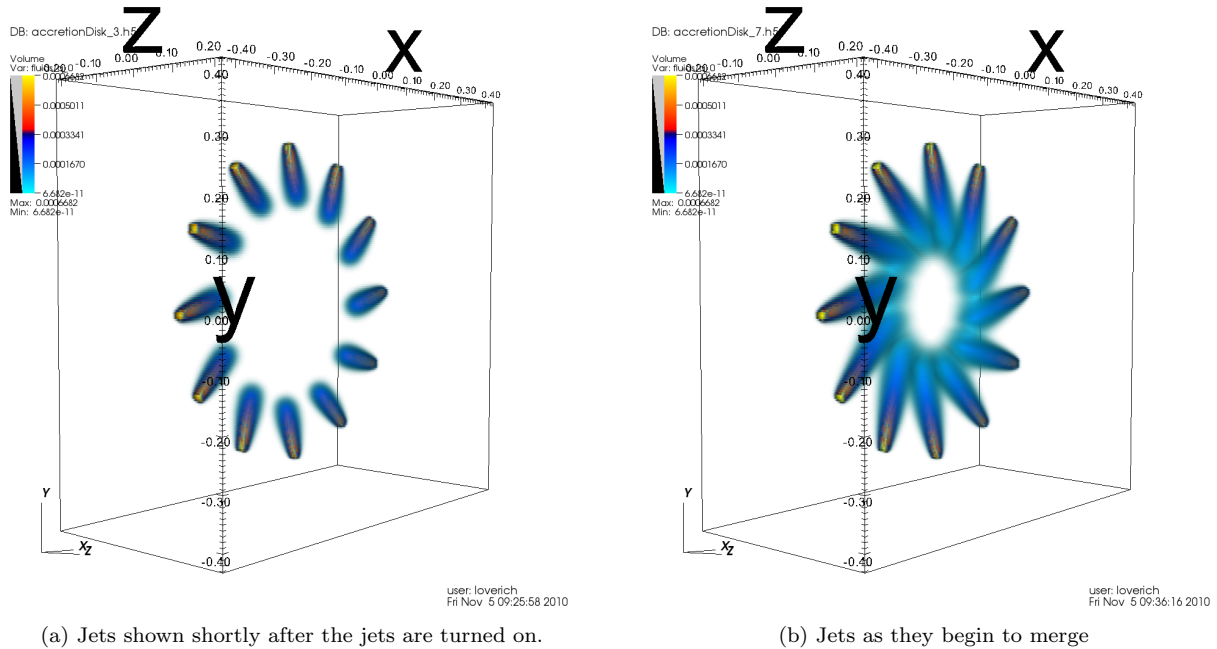
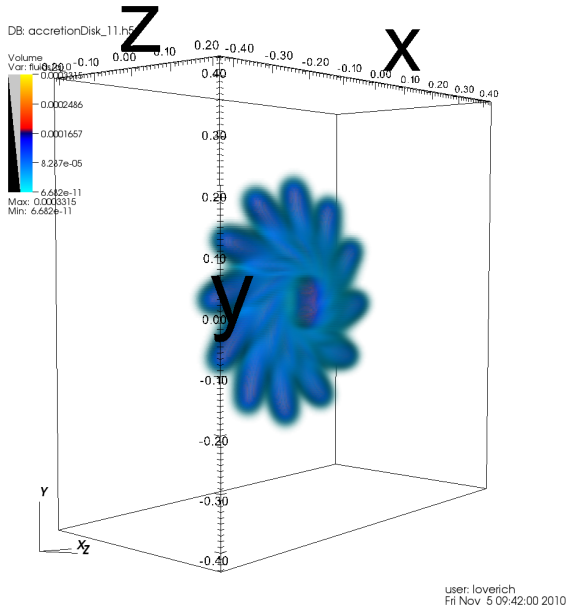
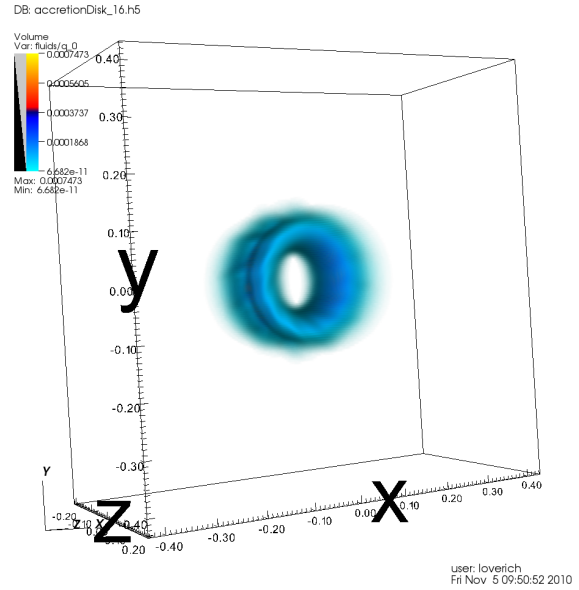


Figure 1: Plasma jets in configuration of accretion disk formation. Plots of argon mass density are shown.

Figures 4-6 show an accretion with field coils turned on. The fields have a strength of 1 Tesla at the center of the field coils and a much lower field in the cusp region. Figure 4 shows the magnetic field lines winding up due to the spinning magnetized fluid as well as density profiles of the jets at the same time. In this case the jets were run continuously instead of being turned off after a few microseconds. Even for continuously running jets the origin remains free of plasma.



(a) Plasma jets after they have finished firing.



(b) Accretion disk as appears a peak density

Figure 2: Plots of argon mass density at 2 different times. The disk never actually collapses on itself in these simulations, however it spins around the axis.

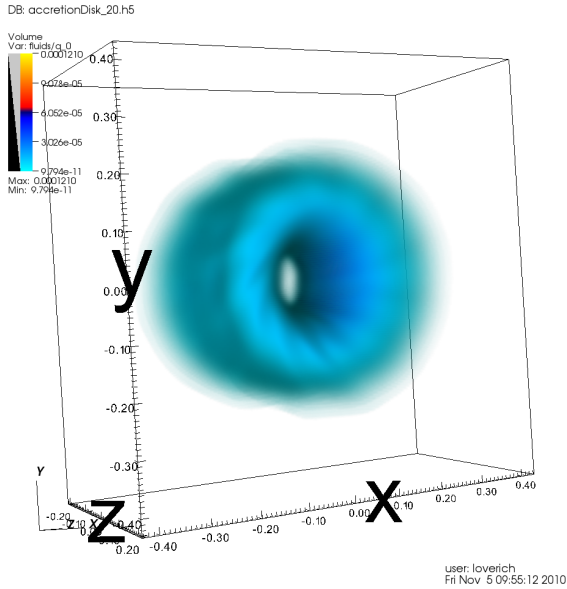
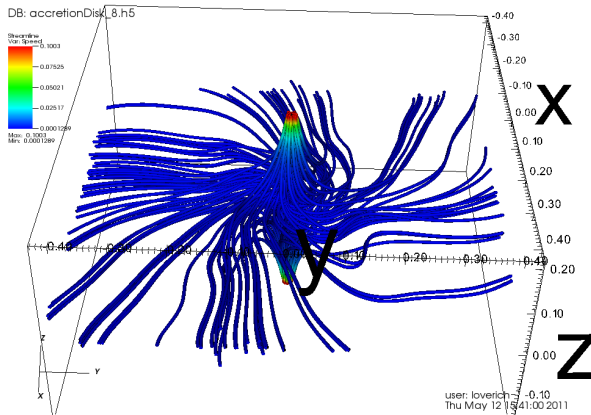
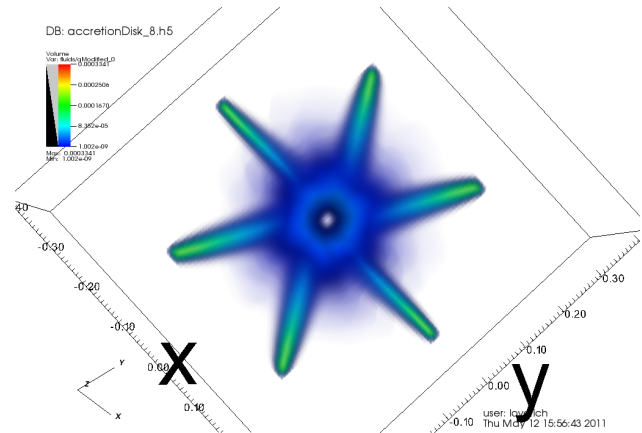


Figure 3: Plot of argon mass density. After 10 microseconds the accretion disk expansion is significant, however a hole remains at the center of the disk.



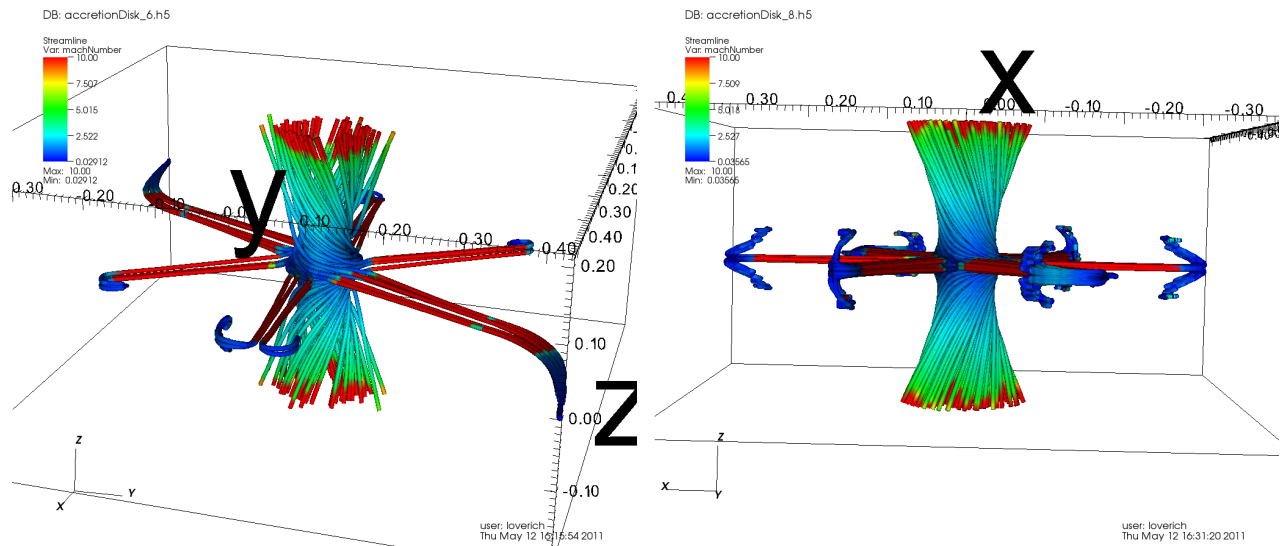
(a) Magnetic field lines of the accretion disk colored by field strength. The field lines show twisting due to the rotation caused by plasma jets.



(b) Top down view of merging plasma jets. The jets are directed slightly off center from the origin by about 6 degrees, this results in a net rotation of the plasma that is visible in the twisting of the magnetic field lines.

Figure 4

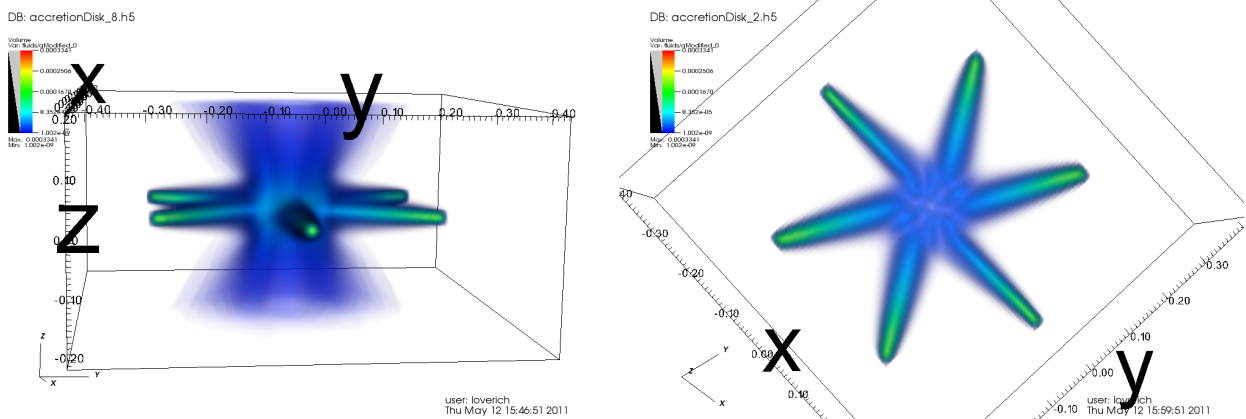
Figure 5 shows velocity streamlines from two different angles. The streamlines are colored by jet Mach number where red is approximately Mach 10 and blue is approximately Mach 0. In these plots the rotation of the fluid is visible as it expands axially in addition to the increase in Mach number. In the merging region of the jets the Mach number drops below Mach 1 (as expected), but then passes through a neck where the flow becomes supersonic. This neck (or nozzle) appears to actually be formed by the fluid itself and not the magnetic field. Plots of magnetic field contours show that the neck in the magnetic field occurs at the center of the field coils (a region not included in the simulations). Furthermore, even running the simulations without magnetic fields shows that supersonic outflow along the axis does develop. However, the presence of a magnetic field results in higher Mach number outflow. All results here are initial and will be investigated in more detail in later work.



(a) Fluid velocity streamlines colored by Mach number. Red indicated Mach 10, the initialized Mach number in the jets. The jets collide resulting in reduced Mach number which then increases as the fluid is expelled perpendicular to the plane of the plasma jets.

(b) Fluid velocity streamlines colored by Mach number. Light blue to red indicate Mach numbers greater than 1. Necking of the fluid flow is observed a short distance from the plane of the merging jets and a subsonic to supersonic transition occurs. Simulations seem to indicate that the magnetic field is not necessary for the supersonic outflow, but it helps to confine the resulting outflow.

Figure 5



(a) Density plot of plasma jets near equilibrium. The merging jets collide and create a conical outflow with low density in the center where the high velocity outflow exists.

(b) Top down view of the merging jets showing some of the shock structure just before the large density outflows begin.

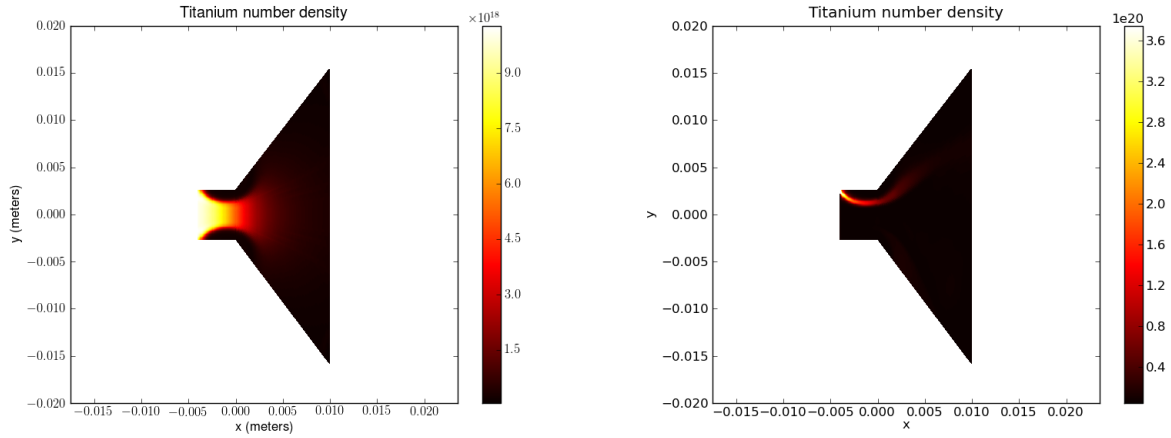
Figure 6

V. Magnetic Nozzle

In a separate project we set up simulations using the split field algorithm to investigate the George Washington University vacuum arc discharge (details can be found in^{9,10}). The discharge can be used to model the plasma environment of a re-entry vehicle and be used to test blackout mitigation techniques. As a first step we've run simple magnetic nozzle simulations assuming uniform discharge. The actual device produces a helical discharge where plasma is transported across field lines to produce a more helical profile. In this case we are simulating a simple magnetic nozzle and then present one simulation where we show two-dimensional spot emission.

To try and mimic the velocities observed in the experiment we've initialized a plasma inflow at 100eV temperatures and a peak magnetic field of around 0.2 tesla at the center of the device. In reality, in ideal MHD the magnitude of the field makes little difference as long as the fluid pressure is much less than the magnetic pressure. When the two are comparable the magnetic field is significantly distorted by the fluid and the field lines act as a flexible (expanding and contracting) nozzle. Using this model the fluid can only move parallel to the field lines and never cross field lines (this is not a restriction of the algorithm this is a restriction of ideal MHD), resistivity and a number of other terms actually allow fluid to cross field lines, but those haven't been included in these simulations.

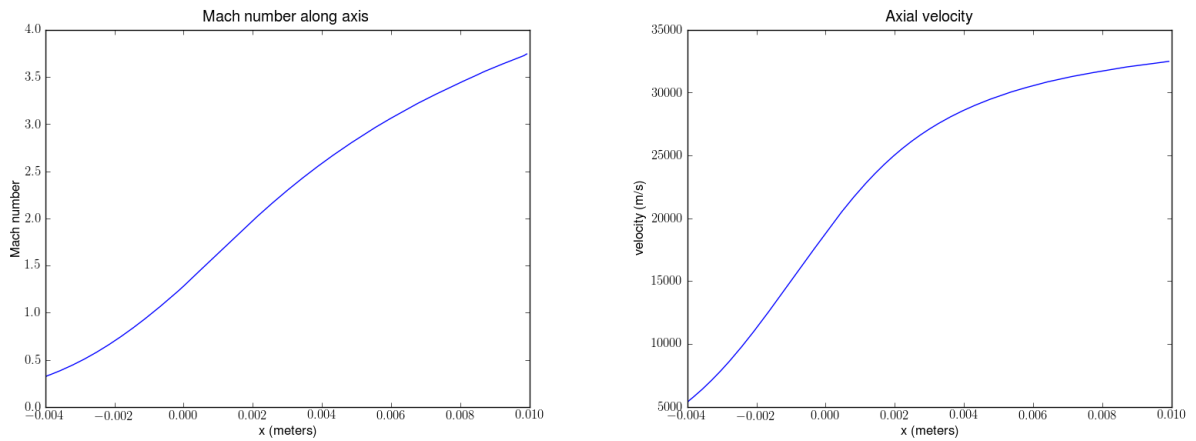
In figure 7a shows density contours of the magnetic nozzle. Fluid is introduced from the left where the velocity is allowed to float. The flow is constricted as the fluid follows the field lines. In figure 8a the axial Mach number is shown. The Mach number starts out subsonic and then transitions to supersonic through the nozzle as would be expected. In figure 8b the axial velocity is shown to reach 33km/s given an initial ion temperature of 100eV. In figure 9a streamlines of the magnetic field for the magnetic nozzle are shown. In figure 9b the streamlines of the velocity are shown. The two sets of streamlines should match closely since in ideal MHD fluid cannot cross field lines. Furthermore, the solution is close to an equilibrium state so the field line streamlines are relatively constant for the duration of a fluid elements passage through the domain of the simulation. Outflow boundary conditions are used on all sides except for the fluid entrance to the domain where a floating velocity is allowed. Figure 7b shows emission from a single spot on the cathode as occurs in the actual experiment. The results show the expansion of the plasma along field lines. In the experiment the emission spot rotates, so an accurate representation of this problem should be done in 3D with the spot rotating, producing a spiraling plasma. Experimentally the plasma appears to occupy a much greater volume, which suggests the importance of a number of other transport effects that have not been included in these simple simulations.



(a) Plot of number density $\frac{\#}{m^3}$ in a magnetic nozzle. All boundary conditions are outflow boundaries (no walls), except at the cathode where a pressure and density are specified. The nozzle is formed by magnetic field lines generated by coils near the exit plane. Simulation includes both induced and perturbed fields so that the fluid pushes back on the magnetic field.

(b) Number density $\frac{\#}{m^3}$ of titanium being emitted from a spot on the cathode. In this case the plasma is confined to a few field lines that pass through the spot. In a configuration like this, the plasma can be used to accelerate a neutral flow as is being pursued in the GWU experiment.

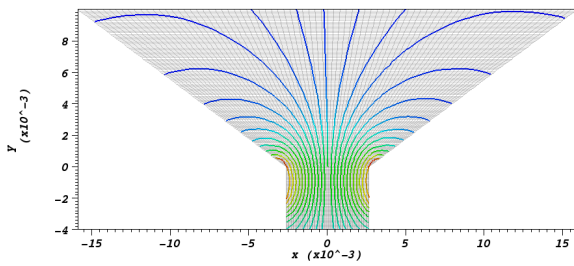
Figure 7



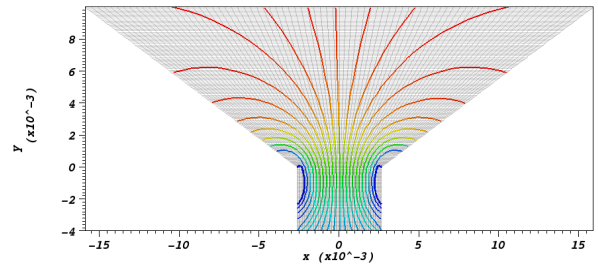
(a) Mach number in the magnetic nozzle based on the acoustic speed. Simulation never quite reaches equilibrium, but the exit Mach number remains above 3. $x=0$ is the location of the right most coil and also marks the transition from subsonic to supersonic flow.

(b) Plot of axial velocity versus axial position. In this case the axial velocity reaches about 33km/s given an initial temperature of 100eV.

Figure 8



(a) Magnetic field lines inside the device. These field lines can be compared to velocity vectors. Ideally they will lay on top of each other, but numerically there may be differences due to numerical diffusion (which results in fluid velocities with components perpendicular to the magnetic field).



(b) Fluid velocity streamlines. Low velocity is indicated by blue and high velocity by red. As the fluid exits the device velocity increases. Velocity vector streamlines seem to do a good job of matching magnetic field streamlines.

VI. Hypersonic blunt body flow

Along the same lines, Tech-X has begun modeling an experiment at George Washington University that uses the plasma source modeled in the previous section. This experiment is set up using the vacuum arc plasma source, where the flow is allowed to pass a mockup of a blunt body. The experiment is meant to simulate conditions of the RAM-IIC re-entry vehicle, but with the ability to modify the conditions to investigate blackout mitigation. The Ram-IIC experiment is a classic experiment used for validation of chemically reacting and ionizing flow. In particular electron densities were measured during the RAM-IIC experiment and can be used to validate numerical codes. Experimental electron density data was taken at several points during the decent of the vehicle, values were calculated based microwave propagation through the air near the vehicle. These experimental measurements can be compared with numerical predictions. A number of researchers have already performed the comparisons, in particular by Candler in.¹¹ In our case weve simplified the problem by using equilibrium specific heats based on the NASA Thermobuild tables, while using non-equilibrium chemistry (rate equations). This misses some key physics for predicting peak temperatures away from the wall, for example the finite electron excitation time means that a lower peak temperature immediately after the shock is observed in our simulations. Nevertheless, electron densities at the wall are on the order of solutions predicted by other computational tools. This capability is important as it will allow Nautilus to predict electron densities along the vehicle which can be used to determine at what conditions, and where, a vehicle will experience radio blackout. The propagation of radio signals through a plasma is directly related to the plasma frequency which is dependent on electron number density.

Figure 9 shows the temperature in the fluid of a blunt body moving at Mach 23 at 61km altitude. Peak temperatures are shown to be 13,500 Kelvin leveling off to around 10,000 Kelvin near the blunt body surface. Peak temperature (just after the shock) is significantly less than predicted by codes that include finite electron excitation time, but agrees after in regions after the shock when full excitation (equilibrium) of the excited states is achieved.

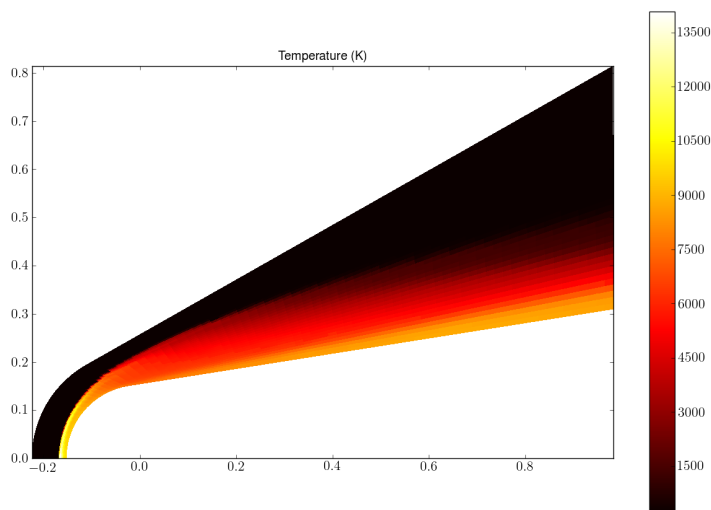


Figure 9: Temperature along re-entry vehicle at 61km altitude

Figure 10a shows species number densities using the 7 species model for the blunt body at 61km altitude moving at Mach 23. N₂ and O₂ dissociate crossing the shock producing, N, O, NO. Ionized NO and electrons are produced near the vehicle body and the electrons are the cause of radio blackout on such a vehicle.

Figure 10b shows similar results but at 71km altitude. At this altitude the finite rate chemistry becomes more important. In all cases a reduced standoff distance (compared to non-reacting flows) is observed as energy is transferred into dissociation and ionization. In these simulations the shock standoff distance is on the order of 1.5cm. Somewhat higher than observed in codes using non-equilibrium specific heats.

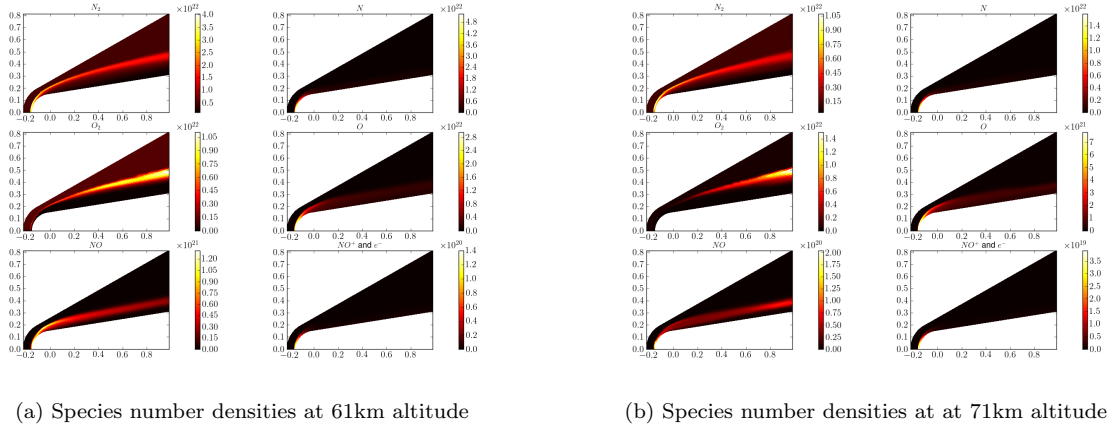


Figure 10

Figure 11 shows the electron density along the surface of the blunt body as measured from the very tip of the vehicle. This parameter is critical for determining what frequency of electromagnetic wave can pass through the plasma, thus determining when and where radio blackout will occur. Given proper modeling of the plasma flow, blackout mitigation techniques can be developed. Michael Keidar has numerically investigated one blackout technique described in.¹² Ultimately this blackout mitigation technique will be investigated in Nautilus.

VII. Conclusion

Tech-X Corporation is currently developing a plasma fluid code that is able to model a broad range of fluid plasma regimes. This paper presents three specific use cases of Nautilus with high speed plasma flow, (a) high density lower temperature weakly ionized air plasmas applicable to hypersonic vehicles (b) high density high temperature regimes with vacuum regions applicable to astrophysical plasmas and (c) magnetic nozzles with applications to thrusters and plasma sources. We are in the process of validating the code with relevant experiments and extending the code to a broader set of problems. For more information and updates on Nautilus visit <http://nautilus.txcorp.com>.

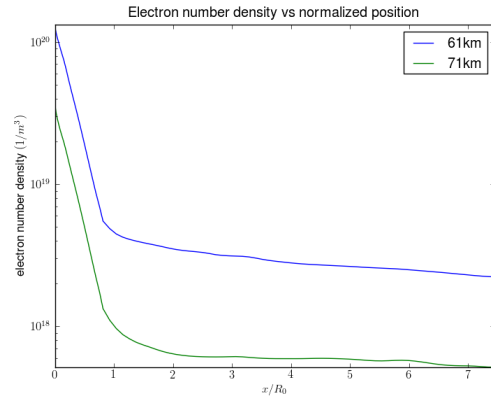


Figure 11: Electron number density measured along the surface of the blunt body. Distance on surface are measured from the tip of the blunt body normalized by the radius of the blunt body cap.

References

- ¹Loverich, J. and Hakim, A., “Two-Dimensional Modeling of Ideal Merging Plasma Jets,” *Journal of Fusion Energy*, 2010, pp. 1–8, 10.1007/s10894-010-9321-z.
- ²Thio, Y. C. F., Knapp, C. E., Kirkpatrick, R. C., Siemon, R. E., and Turchi, P. J., “A Physics Exploratory Experiment on Plasma Liner Formation,” *Journal of Fusion Energy*, Vol. 20, 2001, pp. 1–11, 10.1023/A:1019813528507.
- ³Hsu, S., “Technical Summary of the First U.S. Plasma Jet Workshop,” *Journal of Fusion Energy*, Vol. 28, 2009, pp. 246–257, 10.1007/s10894-008-9162-1.
- ⁴Waagan, K., “A positive MUSCL-Hancock scheme for ideal magnetohydrodynamics,” *Journal of Computational Physics*, Vol. 228, Dec. 2009, pp. 8609–8626.
- ⁵Dedner, A., Kemm, F., Kröner, D., Munz, C.-D., Schnitzer, T., and Wesenberg, M., “Hyperbolic Divergence Cleaning for the MHD Equations,” *Journal of Computational Physics*, Vol. 175, Jan. 2002, pp. 645–673.
- ⁶Witherspoon, F. D., Case, A., Messer, S. J., Bomgardner, R., Phillips, M. W., Brockington, S., and Elton, R., “A contoured gap coaxial plasma gun with injected plasma armature,” *Review of Scientific Instruments*, Vol. 80, No. 8, Aug. 2009, pp. 083506–+.
- ⁷Ryutov, D. D., Plasma Jet Workshop, Los Alamos National Laboratory, Los Alamos, NM, 2008.
- ⁸Ryutov, D. D., “Using intense lasers to simulate aspects of accretion discs and outflows in astrophysics,” *Astrophysics and Space Science*, Dec. 2010, pp. 373–+.
- ⁹Zhuang, T., Shashurin, A., Haque, S., and M., K., “Performance Characterization of the Micro-Cathode Arc Thruster and Propulsion System For Space Applications,” 2010.
- ¹⁰Zhuang, T., Shashurin, A., Keidar, M., and Beilis, I. I., “Circular periodic motion of plasma produced by a small-scale vacuum arc,” *Plasma Sources Science Technology*, Vol. 20, No. 1, Feb. 2011, pp. 015009–+.
- ¹¹Candler, G. V. and MacCormack, R. W., “Computation of weakly ionized hypersonic flows in thermochemical nonequilibrium,” *Journal of Thermophysics and Heat Transfer*, Vol. 5, Sept. 1991, pp. 266–273.
- ¹²Keidar, M., Kim, M., and Boyd, I. D., “Electromagnetic Reduction of Plasma Density During Atmospheric Reentry and Hypersonic Flights,” *Journal of Spacecraft and Rockets*, Vol. 45, May 2008, pp. 445–453.